Draft version November 23, 2017
Preprint typeset using LaTeX style emulateapj v. 01/23/15

DECLINING ROTATION CURVES AT $Z = 2$: A NATURAL PHENOMENON IN ΛCDM COSMOLOGY

Adelheid F. Teklu[1,2], Rhea-Silvia Remus[1,3], Klaus Dolag[1,4], Alexander Arth[1,5], Andreas Burkert[1,5], Aura Obreja[1], & Felix Schulze[1,5]

[1] Universitäts-Sternwarte München, Scheinerstraße 1, D-81679 München, Germany
[2] Excellence Cluster Universe, Boltzmannstraße 2, D-85748 Garching, Germany
[3] Canadian Institute for Theoretical Astrophysics, 60 St. George Street, University of Toronto, Toronto ON M5S 3H8, Canada
[4] Max-Planck Institute for Astrophysics, Karl-Schwarzschild-Str. 1, D-85741 Garching, Germany
[5] Max-Planck Institute for Extraterrestrial Physics, Giessenbachstraße 1, D-85748 Garching, Germany
ateklu@usm.lmu.de

Draft version November 23, 2017

ABSTRACT

Selecting disk galaxies from the cosmological, hydrodynamical simulation *Magneticum Pathfinder* we show that almost half of our poster child disk galaxies at $z = 2$ show significantly declining rotation curves and low dark matter fractions, very similar to recently reported observations. These galaxies do not show any anomalous behavior, reside in standard dark matter halos and typically grow significantly in mass until $z = 0$, where they span all morphological classes, including disk galaxies matching present day rotation curves and observed dark matter fractions. Our findings demonstrate that declining rotation curves and low dark matter fractions in rotation dominated galaxies at $z = 2$ appear naturally within the ΛCDM paradigm and reflect the complex baryonic physics, which plays a role at the peak epoch of star-formation. In addition, we find that dispersion dominated galaxies at $z = 2$, which host a significant gas disk, exhibit similar shaped rotation curves as the disk galaxy population, rendering it difficult to differentiate between these two populations with currently available observation techniques.

Subject headings: dark matter – galaxies: evolution – galaxies: formation – galaxies: halos – hydrodynamics – methods: numerical

1. INTRODUCTION

Since the postulation of dark matter (DM) by Zwicky (1933), many observational studies analyzing rotation curves of galaxies (e.g. Rubin et al. 1978) have supported this picture: While rotational velocities ($V^{\rm rot}$) deduced from the visible matter should decrease proportional to $r^{-1/2}$ in the outer parts of galaxies, they were found to remain flat. The awareness of this discrepancy in the mass content and thus the need for an explanation for this missing mass lead to the acceptance of dark matter as the dominant mass component of galaxies (see Naab & Ostriker (2017) for a detailed review).

Recently, Genzel et al. (2017) (see also Lang et al. 2017) presented measurements of rotation curves at redshift $z \approx 2$ that do not stay flat but decrease with increasing radius, opening a debate about the importance and even presence of DM in the outer disks and inner halos of these massive systems (and generally at higher redshift). In this letter we investigate whether the existence of decreasing rotation curves at high redshifts contradicts or actually is a natural outcome of the ΛCDM paradigm, using the state-of-the-art cosmological simulation Magneticum Pathfinder[1] (K. Dolag et al., in preparation).

2. THE SIMULATIONS

The *Magneticum Pathfinder* simulations are a set of state-of-the-art, cosmological, hydrodynamical simulations of different cosmological volumes with different resolutions. They follow a standard ΛCDM cosmology with parameters (h, Ω_M, Ω_Λ, Ω_b, σ_8) set to (0.704, 0.272, 0.728, 0.0451, 0.809), adopting a WMAP 7 cosmology (Komatsu et al. 2011).

These simulations follow a wide range of physical processes (see Hirschmann et al. 2014; Teklu et al. 2015, for details) which are important for studying the formation of active galactic nuclei (AGN), galaxies, and galaxy cluster. The simulation set covers a huge dynamical range with a detailed treatment of key physical processes that are known to control galaxy evolution, thereby allowing to reproduce the properties of the large-scale, intragalactic, and intra-cluster medium (see e.g. Dolag et al. 2016; Gupta et al. 2017; Remus et al. 2017a) as well as the detailed properties of galaxies including morphological classifications and internal properties (see e.g. Teklu et al. 2015; Remus et al. 2017b; Teklu et al. 2017). This also includes the distribution of different chemical species within galaxies and galaxy clusters (Dolag et al. 2017), and the properties of the AGN population within the simulations (Hirschmann et al. 2014; Steinborn et al. 2016).

For this study we use the simulation *Box4/uhr*, which covers a volume of (68 Mpc)^3, initially sampled with $2 \cdot 576^3$ particles (dark matter and gas), leading to a mass resolution of $m_{\rm gas} = 7.3 \cdot 10^6 M_\odot$ for the gas and $m_{\rm stars} = 1.8 \cdot 10^6 M_\odot$ for stellar particles, with a gravitational softening of $0.7 h^{-1}$kpc.

3. SAMPLE OF GALAXIES

To ensure proper resolution of the inner structure, we only select halos with virial masses above $5 \cdot 10^{11} M_\odot$ hosting galaxies with stellar masses above $5 \cdot 10^{10} M_\odot$ for this study. These mass ranges are consistent with

[1] www.magneticum.org

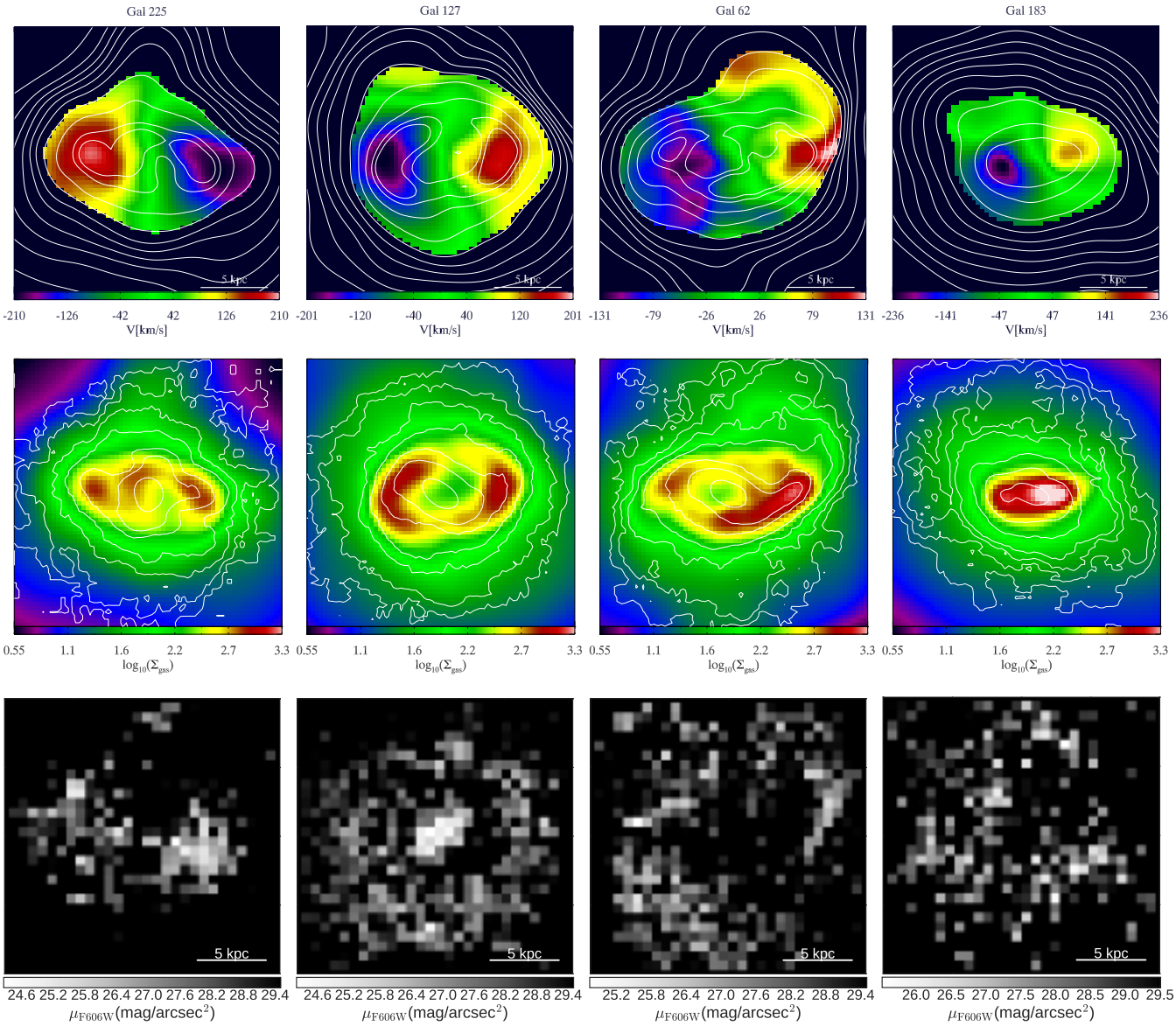

FIG. 1.— Example galaxies from the $z = 2$ sample with declining rotation curves (see Fig. 2), from left to right the three disk galaxies *gal 225*, *gal 127*, and *gal 62*, and the gas-rich spheroidal system *gal 183*, rotated to inclinations (e.g. $i = 60$, $i = 45$, $i = 25$ and $i = 75$, respectively) similar to those of the galaxies presented in Genzel et al. (2017). *Upper row:* Velocity maps of the cold gas component for each galaxy, with contours of the cold gas column density overlayed. *Middle row:* Cold gas column density maps with overlayed stellar column density contours. *Lower row:* Simulated HST broadband F606W images using *GRASIL-3D*.

the observed properties of the high-z galaxy sample of Genzel et al. (2017). This leads to a sample of 212 and 275 halos at $z = 2$ and $z = 0$, respectively. Furthermore, we classifiy the galaxies based on the distribution of the circularity parameter $\varepsilon = j_z/r\sqrt{GM(r)/r}$ of the stars within the galaxies, where j_z is the z-component of the stars' specific angular momentum (see also Abadi et al. 2003; Scannapieco et al. 2008). Thus, dispersion-dominated systems represent observed early-type galaxies and are characterized by a broad peak in the distribution at $\varepsilon \simeq 0$, while rotation-supported systems have properties that are characteristic of late-type galaxies and show a broad peak at $\varepsilon \simeq 1$. We define poster child disk galaxies as systems which, in addition to a characteristic peak at $\varepsilon \simeq 1$, have a significant cold gas fraction ($f_{cold} > 0.5$ at $z = 2$ and $f_{cold} > 0.2$ at $z = 0$) to distinguish them from transition type systems or ongoing merger events (for details see Teklu et al. 2015). For our simulations it has been shown that, following this classification scheme, galaxies of these two populations reproduce accordingly the observed stellar-mass–angular-momentum–relation (Teklu et al. 2015) and its evolution (Teklu et al. 2016), the mass-size relation and its evolution (Remus et al. 2017b), as well as the fundamental plane distributions (Remus & Dolag 2016).

We then rotate the galaxies such that the minor axis of the gas [2] is aligned with the z-axis, so that we can extract the rotation curve without any further modifications.

From the total of 212 (275) galaxies at $z = 2$ ($z = 0$) we classify 26 (15) as poster child disks, which we consider for further analysis. In addition, among our 27 poster

[2] Note that this is different from the computation for the classification, where the galaxies are rotated into the frame where the angular momentum vector of the stars is aligned with the z-axis.

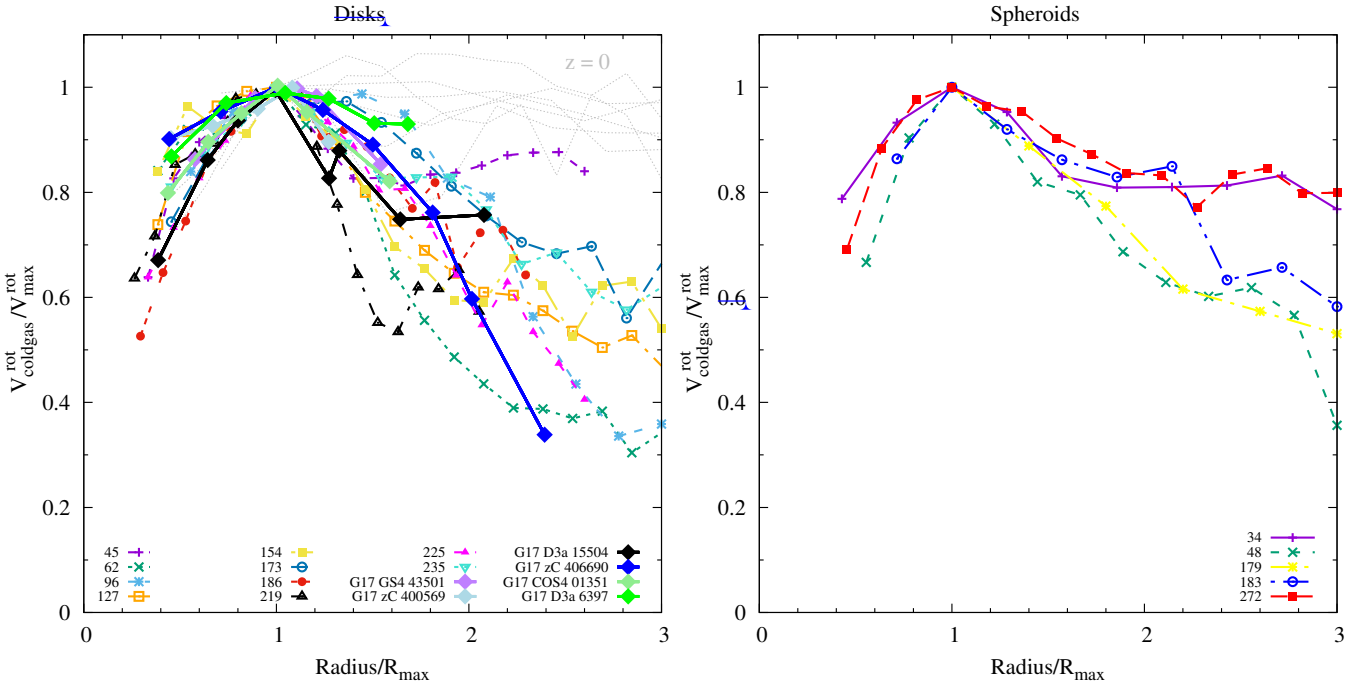

FIG. 2.— Rotation curves obtained from the cold gas for 10 out of the 26 poster child disk galaxies which show clearly declining rotation curves (left panel) and for the 5 gas-rich spheroidal galaxies (right panel) at $z = 2$, normalized by $V^{rot}_{coldgas}$ at the radius of maximum velocity R_{max}. The thick colored lines in the left panel show the 6 declining rotation curves presented in Genzel et al. (2017), while the gray lines show 7 poster child disk galaxies at $z = 0$, using $\approx 1.4 \cdot R_{1/2}$ as R_{max}.

child spheroidal galaxies at $z = 2$ we find 5 systems with a large cold gas fraction ($f_{cold} > 0.5$).

Fig. 1 shows a 20 kpc region for 4 gas-rich example galaxies at $z = 2$, where the upper row displays the line-of-sight velocity maps of the cold gas component, restricted to regions with $\Sigma_{gas} > 50 \frac{M_\odot}{pc^2}$, with overlayed cold gas column density contours. The gridded data was created using SPHMapper (Arth & Roettgers, in prep.). The middle row shows the cold gas column density maps with overlayed stellar surface density contours. Inclinations and colors were chosen according to the observations presented in Genzel et al. (2017). Each column represents one galaxy, where *gal 225*, *gal 127*, and *gal 62* (from left to right) resemble disk galaxies, while *gal 183* is a gas-rich spheroidal galaxy. Interestingly, all galaxies, even the spheroidal one, show a similar, regular rotation pattern for the cold gas component. This is due to the fact that the gas is in a flattened, centrifugally supported disk, while the stars form a spheroid.

The lower panels show mock images of the four galaxies in the HST broadband F606W (4750A-7000A), which corresponds to rest-frame mid-UV. The images have been generated with the radiative transfer code *GRASIL-3D* (Domínguez-Tenreiro et al. 2014). This wavelength range traces the regions of very recent star formation, and the spheroidal galaxy shows a very similar mock image as the disks, hiding the real stellar morphology.

4. ROTATION CURVES AT $Z = 2$

The rotation curves for our galaxy sample are directly obtained from the averaged tangential velocities (i.e. the circular velocities) of the individual cold gas particles. In order to ensure that only gas within the disk contributes to the rotation curve, only particles within the z-range of ±3kpc are used. While the $z = 0$ disk galaxies show normal rotation curves, 12 out of the 26 poster child disk galaxies at $z = 2$ show a significantly declining rotation profile for their gas disk. However, we further remove 2 of the 12 examples from our detailed analysis, as they show remnants of recent merger activity.

The left panel of Fig. 2 shows the rotation curves for these 10 poster child disk galaxies at $z = 2$, which exhibit a decline in the rotation curve similar to the observed high-z disk galaxies presented in Genzel et al. (2017) (thick solid lines). Following the observations, we scaled the individual rotation curves by R_{max} and V^{rot}_{max}, where R_{max} is the radius at which the rotational velocity ($V^{rot}_{coldgas}$) has its maximum. We only plot radii larger than the resolution limit of our simulation, i.e., two times the gravitational softening length of the gas, which corresponds to ≈ 1.33kpc at $z = 2$. As can clearly be seen, the simulated galaxies show the same behaviour as the observed ones, with some having an even steeper decline in the rotation curves as the observed galaxies. For comparison, the rotation curves of 7 disk galaxies at $z = 0$ are shown as gray lines. The difference in profile shapes between high-z and present-day galaxies is clearly visible.

Since at high redshift galaxies are in general more gas-rich, we also plot the same curves for the 5 gas-rich spheroidal galaxies from our $z = 2$ sample in the right panel of Fig. 2. As for the disks, the gas shows a clear rotational pattern (see also example in Fig. 1), and all of our gas-rich spheroidal galaxies show a declining rotation curve similar to the observed disk galaxies. The only difference here is that the gas disks in the spheroidals are much smaller than the stellar spheroidal bodies, while the sizes are similar in the disk galaxy cases (see Fig. 1).

The high redshift HST images mainly show young stars, which morphologically closely resemble the gas

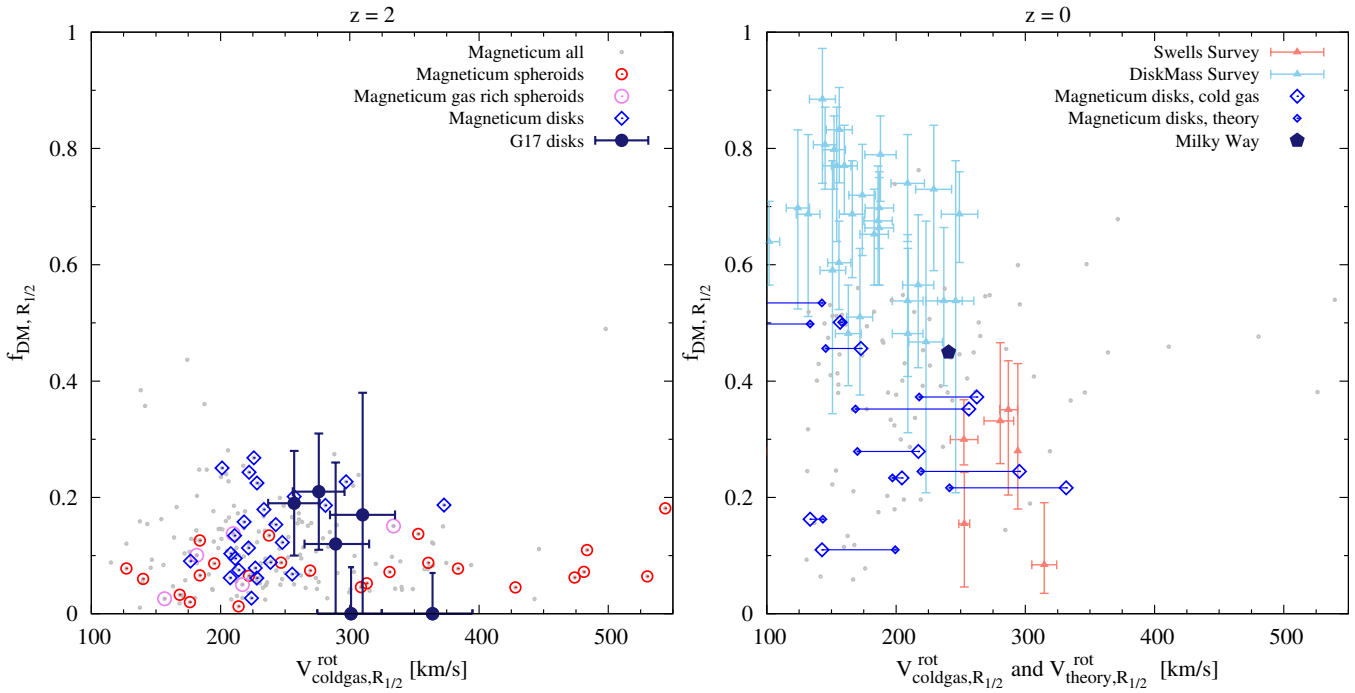

FIG. 3.— The DM fraction $f_{\rm DM}$ within the half-mass radius $R_{1/2}$ versus the rotational velocity $V^{\rm rot}_{\rm coldgas}$ at $R_{1/2}$ at redshifts $z = 2$ (left) and $z = 0$ (right). At $z = 2$ (left panel), the simulated disks (blue diamonds) and gas-rich spheroidals (pink open circles) are shown together with the gas-poor spheroidals (red open circles). The observations from Genzel et al. (2017) are included as dark-blue points. At $z = 0$ (right panel), we only show the simulated disk galaxies, together with observations as presented in Courteau & Dutton (2015) from the Swells Survey (Barnabè et al. 2012; Dutton et al. 2013) and the DiskMass Survey (Martinsson et al. 2013). The dark-blue filled pentagon shows the Milky Way according to Bland-Hawthorn & Gerhard (2016). To indicate uncertainties involved in inferring $V^{\rm rot}_{\rm coldgas,R_{1/2}}$ we include for the simulated galaxies both the measured rotational gas velocity at $R_{1/2}$ as well as the theoretical value obtained from the total mass within $R_{1/2}$ and connect both points by blue lines.

disks even in the spheroidals (see lower panel of Fig. 1). This indicates a potential difficulty in distinguishing disk galaxies from gas-rich spheroidals at $z = 2$ observationally. However, this uncertainty should be resolved using the next generation of telescopes which will be able to probe the old stellar component in high redshift systems as well.

5. DM FRACTIONS

For spheroidal galaxies it is well known that the DM fraction within the half-mass radius is decreasing at higher redshift, which is commonly interpreted as indication for late growth by dry mergers of such systems. While this trend is qualitatively supported by cosmological simulations independent of the details in the implemented feedback models, the AGN feedback used in our simulation has been shown to produce DM fractions which quantitatively agree well with observations (see Remus et al. 2017b).

The left panel of Fig. 3 shows the DM fractions within the stellar half-mass radius $R_{1/2}$ for our full galaxy sample (gray dots) compared to observations at $z = 2$. Generally, our galaxies have a tendency for higher average DM fractions with decreasing $V^{\rm rot}_{\rm coldgas}$, however, nearly all fractions are well below 30%. Our disk galaxies (blue diamonds) cover the same range of small DM fractions as the observations presented in Genzel et al. (2017) (dark-blue filled circles with error bars) [3]. Interestingly, the DM fractions of the disk systems are almost as small as those of the spheroidal systems. Furthermore, the gas-rich spheroidals cover the same range in DM fractions as the observed and simulated disk galaxies, again highlighting the similarities between the gas-rich systems at $z = 2$ independent of their morphologies and demonstrating the difficulty in distinguishing pure rotation-dominated systems from dispersion-dominated systems which host a significant gas disk.

At $z = 0$ the disk galaxies in the simulations show much larger DM fractions which decrease with rotational velocity and agree well with the different measurements for disk galaxies (see right panel of Fig. 3). To indicate uncertainties involved in inferring $V^{\rm rot}_{\rm coldgas,R_{1/2}}$ we used both, the measured rotational gas velocity at $R_{1/2}$ as well as the theoretical values obtained by adopting centrifugal equilibrium and taking the total mass within $R_{1/2}$.

6. SURFACE DENSITY, DISPERSION AND THEORETICAL ROTATION CURVE

A detailed look at the four examples from Fig. 1 shows that the surface density profiles $\Sigma(r)$ of the cold gas disks in the three poster child disk galaxies and the gas-rich spheroidal galaxy follow the expected exponential decline, as shown in the upper panel of Fig. 4. While the theoretical rotation curves as obtained by the total matter distribution within these halos are flat, as expected, the real measured rotation of the cold gas disk shows a significant decline, as can be seen in the middle panel of

[3] Note that especially at $z = 2$ the unavoidable differences when inferring the half-mass radius in simulations and observations could lead to noticeable differences.

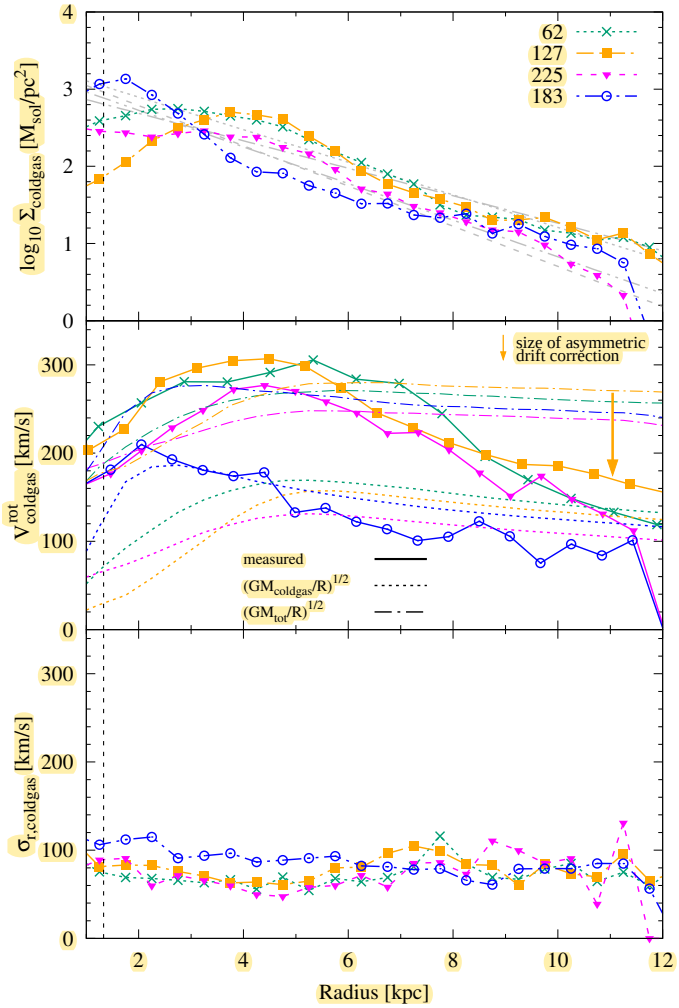

FIG. 4.— For the three poster child disks (*gal 62*, *gal 127*, and *gal 225*), and the gas-rich spheroidal galaxy (*gal 183*): *Upper panel:* Surface density Σ of the cold gas. The vertical dashed line indicates the resolution limit. The gray lines are fits for an exponential surface density profile for $\Sigma(x) = a \cdot exp(-x/b)$ with $b \approx 2$ kpc. *Middle panel:* Rotation curves of the cold gas (solid lines) compared to the rotation curves expected from the spherically averaged total mass distribution (dash-dotted lines). Dotted lines show the corresponding cold gas contribution. The yellow arrow indicates exemplarily the size of the expected correction due to the asymmetric drift at large radii for galaxy *gal 62*. *Bottom panel:* Radial velocity dispersion σ_r of the cold gas.

Fig. 4. This decline is a result of the kinetic pressure effect which partly compensates the gravitational force as proposed by Burkert et al. (2010). As expected for a self-gravitating, exponential disk the maximum of the real rotation curve for the three disk galaxies is slightly ($\approx 10\%$) above the maximum value for a spherically averaged mass distribution. Furthermore, at large distances the real rotational velocity is conspiratorially close to the expected rotational velocity if considering only the cold gas mass. For the gas-rich spheroidal galaxy the latter holds even across almost all radii, due to its even lower DM fraction and the small size of the disk compared to the stellar body of the galaxy. As a result, the gaseous disk is strongly self-gravitating and more compact. None of our systems with a falling rotation curve shows any significant feature or change in the radial component of the velocity dispersion measured for the cold gas disk which is related to the position at which the rotation curve declines, as shown in the σ_r profiles in the lower panel of Fig. 4.

7. DISCUSSION AND CONCLUSIONS

Selecting disk galaxies with $M_{\rm vir}$ above $5 \cdot 10^{11} M_\odot$ and M_* above $5 \cdot 10^{10} M_\odot$ from the cosmological, hydrodynamical simulation *Magneticum Pathfinder* we investigated the rotation curves of disk galaxies at $z = 2$. We find that almost half of our poster child disk galaxies (10 out of 26) show significantly declining rotation curves, very similar to the observations reported in Genzel et al. (2017). Interestingly, the peak of the rotation curve is a fairly good approximation ($\approx 10\%$ larger) of the theoretical value, based on the total mass of the galaxies.

These disk galaxies do not show any significant dynamical features except that the radial dispersion has generally larger values compared to $z = 0$ disks. Applying a simple correction for the asymmetric drift (Burkert et al. 2010) based on our measured dispersion profiles onto the theoretical rotation curve results in reduced rotation curves, which qualitatively agree well with our measured ones. Therefore, we conclude that the declining rotation curves of the high redshift galaxies are caused by a relatively thick, turbulent disk, as already discussed in Genzel et al. (2017). We also find that these galaxies show similarly low DM fractions as reported for the observations. The DM halos of these disk galaxies have a mean concentration parameter $c_{\rm vir} \approx 8$ (as expected for these halo masses at $z = 2$) and therefore we can exclude that the low dark matter fractions are caused by especially low concentrations of the underlying halos.

Tracing these galaxies in the simulations until $z = 0$ allows us to infer the present-day appearances of these galaxies. We find that, on average, these galaxies still grow by a factor of ≈ 3.5 both in virial as well as in stellar mass. Two of them resemble present-day disk galaxies with small remaining gas disks, and one ends as a central galaxy of a small group. Three of them become satellite galaxies of small groups, while the rest is mostly classified as transition types. Therefore, we can exclude that the low DM fractions at $z = 2$ imply that these systems have to be the progenitors of today's elliptical galaxies with similar stellar mass and low dark matter fractions.

Interestingly, in our simulations we also find several spheroidal galaxies at $z = 2$ which host a massive cold gas disk with similarly declining rotation curves as the disk galaxies. These gas disks are typically more compact, but as star formation is dominated by the gas disks, these spheroidals appear indistinguishable from the disk galaxies in our mock HST images, highlighting the need for observational instruments that detect the old stellar component even at high redshifts.

In general, we conclude that high-redshift disk galaxies with declining rotation curves and low DM fractions appear naturally within the ΛCDM paradigm, reflecting the complex baryonic physics which plays a role at $z = 2$ and can be found commonly in state-of-the-art, ΛCDM cosmological hydrodynamical simulations.

We thank Tadziu Hoffmann for useful discussions. AFT and KD are supported by the DFG Transregio TR33, AB is supported by the DFG Priority Programme

1573. AO has been funded by the Deutsche Forschungsgemeinschaft (DFG, German Research Foundation) – MO 2979/1-1. This research is supported by the DFG Cluster of Excellence "Origin and Structure of the Universe." We are especially grateful for the support by M. Petkova through the Computational Center for Particle and Astrophysics (C2PAP). Computations have been performed at the 'Leibniz-Rechenzentrum' with CPU time assigned to the Project "pr86re."

REFERENCES

Abadi, M. G., Navarro, J. F., Steinmetz, M., & Eke, V. R. 2003, ApJ, 597, 21
Barnabè, M., Dutton, A. A., Marshall, P. J., Auger, M. W., Brewer, B. J., Treu, T., Bolton, A. S., Koo, D. C., & Koopmans, L. V. E. 2012, MNRAS, 423, 1073
Bland-Hawthorn, J. & Gerhard, O. 2016, ARA&A, 54, 529
Burkert, A., Genzel, R., Bouché, N., Cresci, G., Khochfar, S., Sommer-Larsen, J., Sternberg, A., Naab, T., Förster Schreiber, N., Tacconi, L., Shapiro, K., Hicks, E., Lutz, D., Davies, R., Buschkamp, P., & Genel, S. 2010, ApJ, 725, 2324
Courteau, S. & Dutton, A. A. 2015, ApJ, 801, L20
Dolag, K., Komatsu, E., & Sunyaev, R. 2016, MNRAS, 463, 1797
Dolag, K., Mevius, E., & Remus, R.-S. 2017, Galaxies, 5, 35
Domínguez-Tenreiro, R., Obreja, A., Granato, G. L., Schurer, A., Alpresa, P., Silva, L., Brook, C. B., & Serna, A. 2014, MNRAS, 439, 3868
Dutton, A. A., Treu, T., Brewer, B. J., Marshall, P. J., Auger, M. W., Barnabè, M., Koo, D. C., Bolton, A. S., & Koopmans, L. V. E. 2013, MNRAS, 428, 3183
Genzel, R., Schreiber, N. M. F., Übler, H., Lang, P., Naab, T., Bender, R., Tacconi, L. J., Wisnioski, E., Wuyts, S., Alexander, T., Beifiori, A., Belli, S., Brammer, G., Burkert, A., Carollo, C. M., Chan, J., Davies, R., Fossati, M., Galametz, A., Genel, S., Gerhard, O., Lutz, D., Mendel, J. T., Momcheva, I., Nelson, E. J., Renzini, A., Saglia, R., Sternberg, A., Tacchella, S., Tadaki, K., & Wilman, D. 2017, Nature, 543, 397
Gupta, N., Saro, A., Mohr, J. J., Dolag, K., & Liu, J. 2017, MNRAS, 469, 3069
Hirschmann, M., Dolag, K., Saro, A., Bachmann, L., Borgani, S., & Burkert, A. 2014, MNRAS, 442, 2304
Komatsu, E., Smith, K. M., Dunkley, J., Bennett, C. L., Gold, B., Hinshaw, G., Jarosik, N., Larson, D., Nolta, M. R., Page, L., Spergel, D. N., Halpern, M., Hill, R. S., Kogut, A., Limon, M., Meyer, S. S., Odegard, N., Tucker, G. S., Weiland, J. L., Wollack, E., & Wright, E. L. 2011, ApJS, 192, 18
Lang, P., Förster Schreiber, N. M., Genzel, R., Wuyts, S., Wisnioski, E., Beifiori, A., Belli, S., Bender, R., Brammer, G., Burkert, A., Chan, J., Davies, R., Fossati, M., Galametz, A., Kulkarni, S. K., Lutz, D., Mendel, J. T., Momcheva, I. G., Naab, T., Nelson, E. J., Saglia, R. P., Seitz, S., Tacchella, S., Tacconi, L. J., Tadaki, K.-i., Übler, H., van Dokkum, P. G., & Wilman, D. J. 2017, ApJ, 840, 92
Martinsson, T. P. K., Verheijen, M. A. W., Westfall, K. B., Bershady, M. A., Andersen, D. R., & Swaters, R. A. 2013, A&A, 557, A131
Naab, T. & Ostriker, J. P. 2017, ARA&A, 55, 59
Remus, R.-S. & Dolag, K. 2016, in The Interplay between Local and Global Processes in Galaxies,
Remus, R.-S., Dolag, K., & Hoffmann, T. 2017a, Galaxies, 5, 49
Remus, R.-S., Dolag, K., Naab, T., Burkert, A., Hirschmann, M., Hoffmann, T. L., & Johansson, P. H. 2017b, MNRAS, 464, 3742
Rubin, V. C., Thonnard, N., & Ford, Jr., W. K. 1978, ApJ, 225, L107
Scannapieco, C., Tissera, P. B., White, S. D. M., & Springel, V. 2008, MNRAS, 389, 1137
Steinborn, L. K., Dolag, K., Comerford, J. M., Hirschmann, M., Remus, R.-S., & Teklu, A. F. 2016, MNRAS, 458, 1013
Teklu, A. F., Remus, R.-S., & Dolag, K. 2016, in The Interplay between Local and Global Processes in Galaxies,
Teklu, A. F., Remus, R.-S., Dolag, K., Beck, A. M., Burkert, A., Schmidt, A. S., Schulze, F., & Steinborn, L. K. 2015, ApJ, 812, 29
Teklu, A. F., Remus, R.-S., Dolag, K., & Burkert, A. 2017, MNRAS, 472, 4769
Zwicky, F. 1933, Helvetica Physica Acta, 6, 110

Mon. Not. R. Astron. Soc. **000**, 000–000 (0000) Printed November 29, 2017 (MN LATEX style file v2.2)

Digging for red nuggets: discovery of a hot halo surrounding a massive, compact relic galaxy

N. Werner[1,2,3⋆], K. Lakhchaura[1], R. E. A. Canning[4]†, M. Gaspari[5]‡, A. Simionescu[6]
[1]*MTA-Eötvös University Lendület Hot Universe Research Group, Pázmány Péter sétány 1/A, Budapest, 1117, Hungary*
[2]*Department of Theoretical Physics and Astrophysics, Faculty of Science, Masaryk University, Kotlářská 2, Brno, 611 37, Czech Republic*
[3]*School of Science, Hiroshima University, 1-3-1 Kagamiyama, Higashi-Hiroshima 739-8526, Japan*
[4]*Kavli Institute for Particle Astrophysics and Cosmology, Stanford University, 452 Lomita Mall, Stanford, CA 94305-4085, USA*
[5]*Department of Astrophysical Sciences, Princeton University, 4 Ivy Lane, Princeton, NJ 08544-1001, USA*
[6]*Institute of Space and Astronautical Science (ISAS), JAXA, 3-1-1 Yoshinodai, Chuo-ku, Sagamihara, Kanagawa, 252-5210, Japan*

November 29, 2017

ABSTRACT

We present the results of a *Chandra* X-ray observation of the massive relic galaxy Mrk 1216, a present day red nugget. Compact massive galaxies with $r_e \lesssim 2$ kpc and $M_\star \gtrsim 10^{11}\ M_\odot$ observed at $z > 2$, also called red nuggets, formed in quick dissipative events and later grew by a series of dry mergers into the local giant ellipticals. Due to the stochastic nature of mergers, a few of the primordial massive galaxies avoided the mergers and remained untouched over cosmic time. Here we report the first detection of an X-ray emitting atmosphere surrounding such a relic galaxy. The hot atmosphere extends far beyond the stellar population and has an 0.5–7 keV X-ray luminosity of $L_X = (6.9 \pm 0.9) \times 10^{41}$ erg s^{-1}, which is similar to typical giant ellipticals. The hot gas has a short cooling time of ~ 45 Myr and the galaxy has a ~ 13 Gyr old stellar population. The presence of an X-ray atmosphere with a short nominal cooling time and the lack of young stars indicate the presence of a sustained heating source, which prevented star formation since the dissipative origin of the galaxy 13 Gyrs ago. The central temperature peak and the presence of radio emission in the core of the galaxy indicate that the heating source is radio-mechanical AGN feedback. The presence of hot atmospheres around massive galaxies in the early universe has important consequences for studies of galaxy quenching and maintenance mode feedback.

Key words: galaxies: evolution – galaxies: formation – galaxies: active – X-rays: galaxies

1 INTRODUCTION

The formation and evolution of giant elliptical galaxies is well described by two-phase models (Oser et al. 2010; Rodriguez-Gomez et al. 2016). The first phase is a quick dissipative event, when the core of the galaxy and its supermassive black hole are formed. The results of this first stage are the compact massive galaxies with $r_e \lesssim 2$ kpc and $M_\star \gtrsim 10^{11}\ M_\odot$, so called red nuggets observed at $z > 2$. This early growth is followed by a slow accretion phase when the galaxy undergoes dry mergers with lower mass galaxies. These random encounters will place most of the newly accreted material at the periphery of the galaxy, significantly increasing its size, but leaving the centre unaffected. Semi-analytical models and cosmological simulations indicate that the size of a massive galaxy can increase by a factor of ~ 7 during the merger phase, while its velocity dispersion increases by at most a factor ~ 1.1 (Hilz et al. 2012). However, due to the stochastic nature of mergers, a few of the primordial massive galaxies should avoid the second stage, remaining untouched over cosmic time (Quilis & Trujillo 2013).

The first confirmed low redshift *massive relic galaxy*, mimicking the properties of high-redshift compact massive galaxies, is NGC 1277 ($r_e = 1.2$ kpc and $M_\star = 1.3 \times 10^{11}\ M_\odot$) in the Perseus cluster (Trujillo et al. 2014). This galaxy is also well known for hosting an over-massive black hole (van den Bosch et al. 2012). Ferré-Mateu et al. (2015) identified a sample of seven potential massive relic galaxies, all with unusually massive central black holes (3–5σ outliers on the $M_{BH} - M_{bulge}$ relation). Recently, Ferré-Mateu et al. (2017) confirmed that two previously identified candidates (MRK 1216 and PGC 032873) are indeed "red nuggets" in the present day Universe (see also Walsh et al. 2017). The stellar populations of these galaxies are highly concentrated in the innermost parts, they were formed quickly and early, and their mean mass-weighted ages are ~ 13 Gyr. They have strongly peaked velocity dispersion profiles with high radial velocities, and compact and elongated morphologies with no signs of interactions. These properties set them clearly apart from typical giant ellipticals; in-

⋆ wernernorbi@gmail.com
† *Einstein* Fellow
‡ *Einstein* and *Spitzer* Fellow

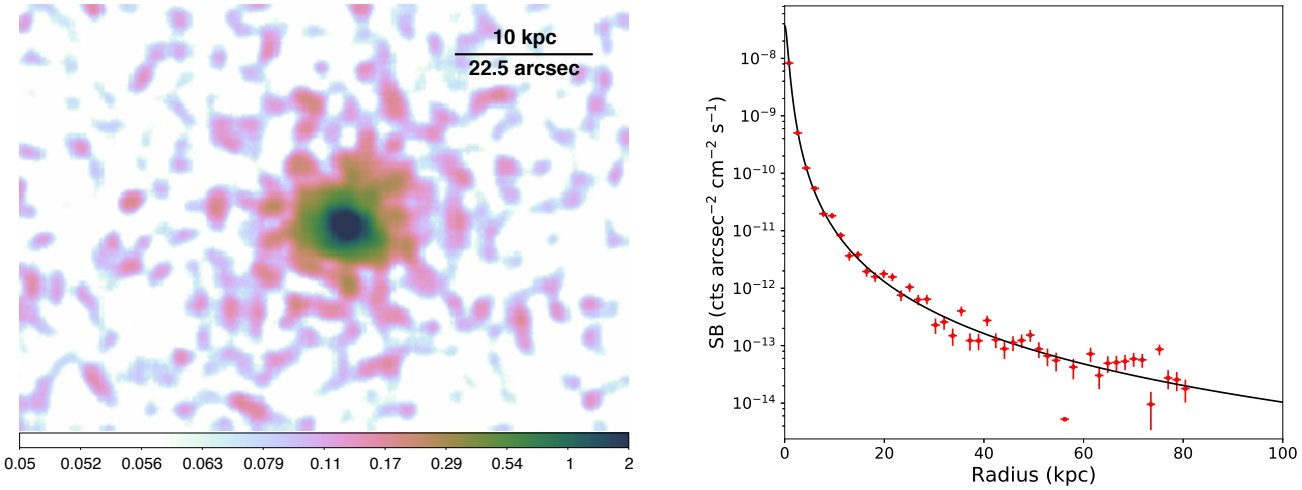

Figure 1. *Left panel:* The *Chandra* X-ray data reveal a hot X-ray emitting atmosphere around the isolated, massive, compact, relic galaxy Mrk 1216. *Right panel:* The X-ray surface brightness profile shows that the X-ray emitting atmosphere of this relic galaxy extends far beyond its stellar population, out to radii of 55 kpc. The emission is fit with a beta model of $\beta = 0.66 \pm 0.15$ and $r_c = 0.7 \pm 0.1$ kpc.

stead, they represent the properties of the early population of red nuggets observed at redshifts $z \gtrsim 2$ (e.g. Buitrago et al. 2008; van der Wel et al. 2011), that only went though the first dissipative phase of galaxy formation. These systems thus allow us to perform a detailed study of red nuggets, the puzzling progenitors of giant elliptical galaxies.

If red nuggets are indeed progenitors of giant elliptical galaxies, then we might expect them to host hot X-ray emitting atmospheres. The presence of hot atmospheres around massive galaxies in the early universe would have important consequences for studies of galaxy quenching and maintenance mode feedback. The X-ray morphologies, thermodynamic properties, and metallicities of these atmospheres will also carry important information about the more recent growth and evolution of these systems. The most isolated of the three currently confirmed low redshift massive relic galaxies is MRK 1216 ($z = 0.021328$, $D = 113$ Mpc), with only two nearby galaxies at distance $\gtrsim 1$ Mpc. Therefore, this system provides the best opportunity for the study of extended X-ray emitting haloes around red nuggets, long before future large X-ray missions, such as *Athena* or *Lynx*, will allow us to observe the massive high redshift galaxies directly.

2 OBSERVATIONS AND DATA ANALYSIS

MRK 1216 has been observed by *Chandra* for 12.9 ks in June 2015 using the Advanced CCD Imaging Spectrometer (ACIS) chip 6. We analysed these archival data using standard data analysis procedures (e.g. Lakhchaura et al. 2016; Werner et al. 2014, 2016). Background images were extracted from the blank-sky fields available from the Chandra X-ray Center. These were cleaned in an identical way to the source observations, reprojected to the same coordinate system and normalized by the ratio of the observed to blank-sky count rates in the 9.5–12 keV band. For spectroscopy we used a local background extracted from the same chip as the source spectrum.

We modelled the spectra of MRK 1216 as absorbed single-phase plasma in collisional ionisation equilibrium (CIE), with the temperature, spectral normalisation and metallicity as free parameters, and a $kT = 7.3$ keV bremsstrahlung model with a free normalisation to account for the population of unresolved galactic point sources (Irwin et al. 2003; Boroson et al. 2011). The normalisation of the unresolved point source component has large errors and is not statistically significant in the fits of MRK 1216. The line-of-sight absorption column density was fixed to the value $N_H = 4.03 \times 10^{20}$ cm^{-2} determined by the Leiden/Argentine/Bonn radio survey of H I (Kalberla et al. 2005).

To determine the azimuthally averaged, deprojected radial profiles of thermodynamic quantities, we extracted spectra from five concentric annular regions. We modelled the spectra using the PROJCT model implemented in the XSPEC spectral fitting package (Arnaud 1996). The combined set of spectra was modelled in the 0.6–7.0 keV band simultaneously to determine the deprojected electron density (n_e) and temperature (kT) profiles. From the electron densities and temperatures we determined the entropy, $K = kT_e/n_e^{\frac{2}{3}}$, and cooling time, $t_{cool} = \frac{3}{2}(n_e + n_i)kT/(n_e n_i \Lambda(T))$, profiles, where the ion number density $n_i = 0.92 n_e$, and $\Lambda(T)$ is the cooling function for Solar metallicity tabulated by Schure et al. (2009).

3 RESULTS

The *Chandra* X-ray observation revealed a gaseous X-ray halo surrounding MRK 1216, extending far beyond its stellar population (see Fig. 1). The X-ray emission is detected with a significance greater than 3σ out to a radius of 55 kpc. The spectrum of the central region is entirely consistent with thermal emission. The upper limit on the 0.5–7 keV X-ray luminosity of a power-law like emission component from the active galactic nucleus (AGN) and possibly unresolved point sources within the radius of 1 kpc is 9.47×10^{39} erg s^{-1}, which is about 3.4 per cent of the thermal emission in this region. The total 0.5–7 keV X-ray luminosity within the radius of 10 kpc is $L_X = (6.9 \pm 0.9) \times 10^{41}$ erg s^{-1}, which is similar to the luminosities of the hot atmospheres of giant ellipticals (e.g. Werner et al. 2014).

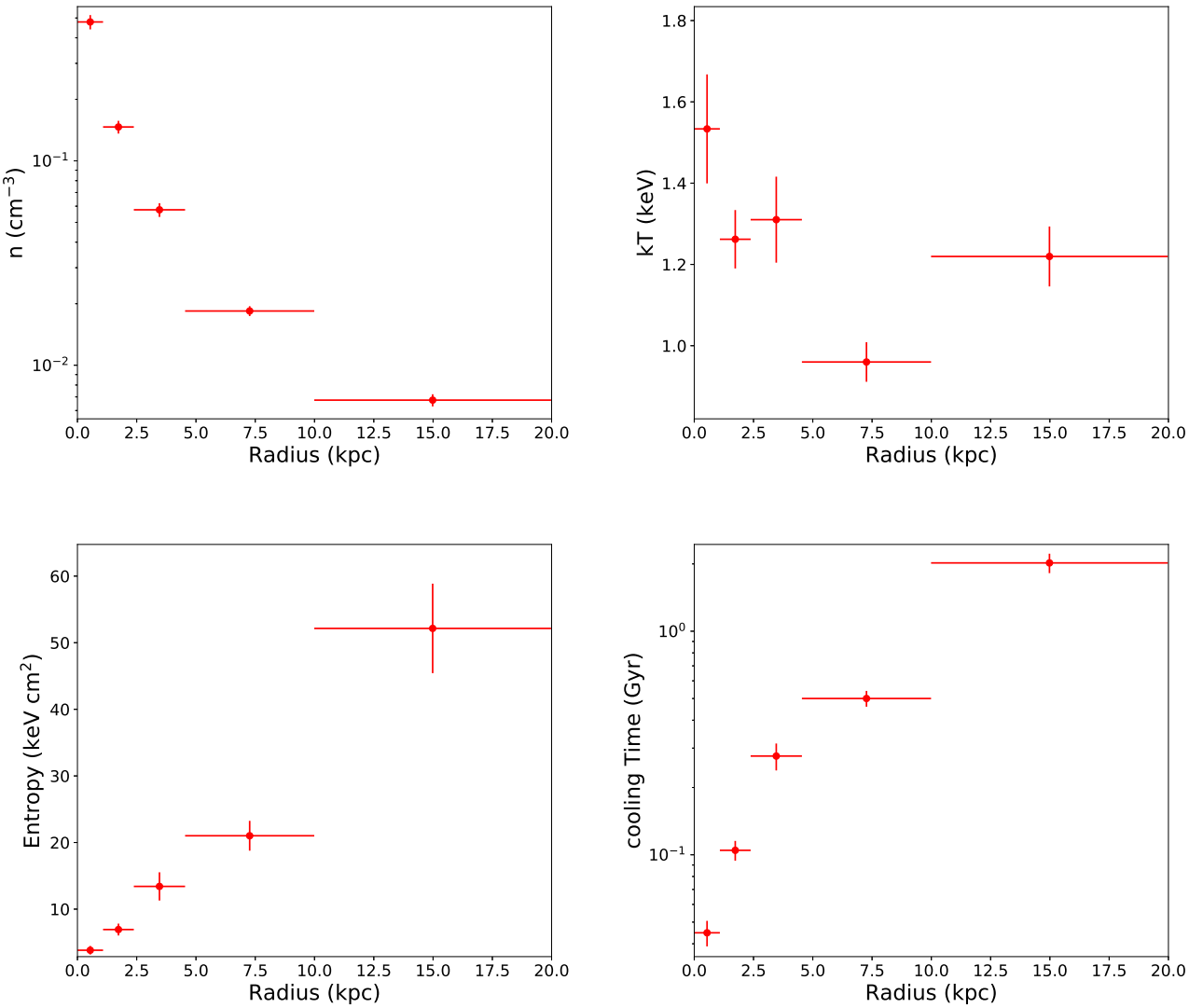

Figure 2. Radial distributions of the deprojected thermodynamic properties of the X-ray emitting atmosphere of the massive relic galaxy Mrk 1216: total density $n = n_e + n_i$ (top left), temperature (top right), entropy (bottom left), and cooling time (bottom right).

By fitting a model of a single-temperature plasma in collisional ionisation equilibrium to the global spectrum extracted within the radius of $r = 4.4$ kpc, we determine a best fit metallicity of 0.7 ± 0.2 Solar (assuming the Solar abundances of Lodders & Palme 2009). This metallicity is likely to be biased low due to an intrinsically multi-temperature structure of the gas (see Buote 2000; Werner et al. 2008). The low photon statistics does, unfortunately, not allow us to place meaningful constraints on the multi-temperature structure.

The data allow us to determine the radial distribution of azimuthally averaged spectral properties in five concentric annuli (see Fig. 2). The galaxy has a relatively high central density of $n = 0.48 \pm 0.04$ cm^{-3}, a centrally peaked temperature distribution (core temperature of $kT = 1.53 \pm 0.13$ keV), a relatively flat entropy profile with a power-law index of 0.78 ± 0.06, and a cooling time of $t_{\rm cool} = 44.8 \pm 5.8$ Myr. The short cooling time means that unchecked radiative cooling would lead to reservoirs of cold gas and star formation. If we fit the spectra with a simple isobaric cooling flow model (although in reality the presence of simple isobaric cooling is unlikely), we obtain a mass deposition rate between 0.1 keV and 1.2 keV of $\dot{M} = 1.18 \pm 0.14\ M_\odot$ yr^{-1}. Taken together with the old stellar population of the galaxy (mean mass weighted age of 12.8 ± 1.5 Gyr, with 99% of the stellar population more than 10 Gyrs old; Ferré-Mateu et al. 2017), the short cooling time implies the presence of a heating source, which prevents the radiative cooling of the halo. The temperature distribution is strongly centrally peaked consistent with the presence of a nuclear heating source. The presence of ionised gas has not been reported for this system. The Very Large Array (VLA) FIRST survey (Condon et al. 1998) shows a central radio source in the galaxy, with a flux of 9.2 ± 0.6 mJy at 1.4 GHz, corresponding to a radio luminosity of 1.9×10^{38} erg s^{-1}.

The total hot gas mass within the radius of $r < 10$ kpc is $M_{\rm gas} = 1.4 \pm 0.06 \times 10^9\ M_\odot$, comparable to the gas mass in nearby giant ellipticals (e.g. Werner et al. 2014). The gas mass is a small fraction of the stellar mass, which is $M_\star = (2.0 \pm 0.8) \times 10^{11}\ M_\odot$.

The total mass within the same radius, calculated from the pressure profile assuming hydrostatic equilibrium, is $M_{\rm tot} = (7\pm5)\times10^{11}\ M_\odot$, consistent with the dynamical mass of the system (see Yıldırım et al. 2015). The gas mass fraction is within the range measured in the nearby, mature, massive elliptical galaxies (Werner et al. 2012).

4 DISCUSSION

MRK 1216, an isolated, massive, compact relic galaxy, harbours a hot X-ray emitting atmosphere, extending far beyond its stellar population. The galaxy has likely been holding on to its hot gas since its formation $\sim$ 13 Gyr ago. The presence of an X-ray emitting atmosphere in this relic system suggests that red nuggets observed at high redshifts are very likely to host X-ray atmospheres as well.

Hot atmospheres might be leftover material from the process of galaxy formation and stellar mass loss may also have contributed significantly to the X-ray emitting gas mass (for a review see Mathews & Brighenti 2003). Hydrodynamic simulations predict that about 75 per cent of the ejecta produced by red giant stars moving supersonically relative to the ambient medium will be shock heated to approximately the temperature of the hot gas (Parriott & Bregman 2008; Bregman & Parriott 2009). The evolved stellar population of the galaxy is expected to contribute $\sim$ 1 $M_\odot$ yr^{-1} per 10^{11} $M_\odot$ (Canning et al. 2013), which means that at the current mass loss rate the amount of gas within the inner 10 kpc of the atmosphere could be built up in less than 1 Gyr. The surface brightness, density and temperature profiles do not show the presence of abrupt jumps, indicating that the atmosphere of this isolated galaxy is continuous. We note that various parts of the hot gaseous atmosphere, with increasing radius, could in principle be labeled as inter-stellar medium (ISM), circum-galactic medium (CGM), and intergalactic medium (IGM).

The presence of an X-ray atmosphere with a short nominal cooling time and the lack of young stars indicate the presence of a sustained heating source, which prevented star formation for 13 Gyrs, since the quick dissipative formation of the galaxy. The central temperature peak, the relatively flat entropy profile (index of 0.78 ± 0.06, which is flatter than the value of $\sim$ 1.1 expected from gravitational collapse; Voit et al. 2005) and the presence of a radio source in the core of the galaxy indicate that, similarly to cooling core clusters and giant ellipticals, the heating source is radio-mechanical AGN feedback (for review see McNamara & Nulsen 2007, 2012). The cooling time over free-fall time $t_{\rm cool}/t_{\rm ff} \sim 20$ within the central $r \lesssim 10$ kpc of MRK 1216 is also similar to the values measured in the centres of many clusters, groups and giant elliptical galaxies (Hogan et al. 2017; Pulido et al. 2017). The radially decreasing temperature profile is consistent with compressional heating in a steep central gravitational potential in the presence of sustained gentle heating (see e.g. Gaspari et al. 2012). Similarly to the brightest cluster galaxies of luminous cooling core clusters (Hlavacek-Larrondo & Fabian 2011; Russell et al. 2013) and nearby giant ellipticals (Werner et al. 2012, 2014), the AGN with an X-ray luminosity $L_{\rm X} < 9.47\times10^{39}$ erg s^{-1} is accreting at a very small Eddington ratio of $L_{\rm X}/L_{\rm Edd.} \lesssim 10^{-8}$. The radio luminosity is also similar to the giant ellipticals with ongoing radio-mechanical AGN feedback.

The black hole mass of $M_{\rm BH} = (4.9 \pm 1.7) \times 10^9\ M_\odot$ in MRK 1216 is a factor of 5–10 larger than the expectations from the black hole mass–bulge mass relation established at $z = 0$ (Walsh et al. 2017; Ferré-Mateu et al. 2017). This relic galaxy avoided the accretion of stellar material through mergers, but its black hole could have reached a significant fraction of its current mass during the early stages of the fast dissipative growth. However, an appreciable fraction of the black hole mass could also have been accreted from the hot X-ray emitting halo. Gaspari & Sądowski (2017) show that the accretion rate onto the supermassive black hole is tightly linked to the X-ray luminosity of the plasma halo, since it is the progenitor source for the feeding mechanism. Multiphase gas condenses out of the hot halo (Gaspari et al. 2017), raining onto the central region, and through inelastic collisions the cold/warm clouds are rapidly funnelled toward the central black hole, in a physical process called chaotic cold accretion (Gaspari et al. 2013). Therefore, while red nuggets may have a small stellar mass, the extended halo mass can provide the fuel to help grow the unusually massive black holes seen in these relic galaxies. Recently, it has been suggested that the total halo mass, and thus the X-ray gas luminosity, correlates better with the black hole mass than the stellar populations of the host galaxies (Bogdán et al. 2012; Bogdán & Goulding 2015). The study of the X-ray emitting gas in massive relic galaxies could therefore be crucial to advance our knowledge of AGN feeding and feedback at the different evolutionary stages of giant ellipticals.

MRK 1216 is a fast rotating galaxy ($v_{\rm r} = 180$ km s^{-1}; Ferré-Mateu et al. 2017) and therefore its hot atmosphere is also expected to have a significant angular momentum. In the case of a low turbulence, for edge-on galaxies the rotation would introduce an ellipticity of $\epsilon \sim 0.7-0.8$ (see Brighenti et al. 2009). For outflowing or turbulent hot gas the ellipticity would be significantly lower. The fact that we do not detect departures from spherical symmetry could be related to AGN induced turbulent motions in the atmosphere. An in-depth study of the shape of the extended hot halo will require deeper X-ray observations of this unique galaxy.

5 CONCLUSIONS

Here we report the first detection of a hot X-ray emitting atmosphere around an isolated, massive, compact, relic galaxy. The 0.5–7 keV X-ray luminosity of $L_{\rm X} = (6.9 \pm 0.9) \times 10^{41}$ erg s^{-1} and the gas mass of $M_{\rm gas} = (1.4 \pm 0.06) \times 10^9\ M_\odot$ within $r < 10$ kpc are similar to typical giant ellipticals.

- The galaxy shows a high central density of $n = 0.48 \pm 0.04$ cm^{-3}, a central temperature peak of $kT = 1.53 \pm 0.13$ keV, a short cooling time of $t_{\rm cool} = 44.8 \pm 5.8$ Myr, and a $\sim$ 13 Gyr old stellar population. The presence of an X-ray atmosphere with a short nominal cooling time and the lack of young stars indicate the presence of a sustained heating source, which prevented star formation since the dissipative formation of the galaxy 13 Gyrs ago. The central temperature peak, the presence of radio emission in the core of the galaxy, and the low Eddington ratio indicate that the heating source is radio-mechanical AGN feedback.
- MRK 1216 is a strong outlier from the black hole mass–bulge mass relation at $z = 0$. An appreciable fraction of the black hole mass could have been accreted from the hot X-ray emitting halo, as suggested by theoretical predictions of chaotic cold accretion. The study of the X-ray emitting gas in massive relic galaxies could therefore be crucial to advance our knowledge of AGN feeding and feedback at the different evolutionary stages of massive galaxies.

ACKNOWLEDGMENTS

This work was supported by the Lendület LP2016-11 grant awarded by the Hungarian Academy of Sciences. M. G. thanks Fabrizio Brighenti for insightful discussions. M. G. is supported by NASA through Einstein Postdoctoral Fellowship Award Number PF5-160137 issued by the Chandra X-ray Observatory Center, which is operated by the SAO for and on behalf of NASA under contract NAS8-03060. Support for this work was also provided by Chandra grant GO7-18121X.

REFERENCES

Arnaud K. A., 1996, in Astronomical Data Analysis Software and Systems V, edited by G. H. Jacoby, J. Barnes, vol. 101 of Astronomical Society of the Pacific Conference Series, 17
Bogdán Á., Forman W. R., Zhuravleva I., et al., 2012, ApJ, 753, 140
Bogdán Á., Goulding A. D., 2015, ApJ, 800, 124
Boroson B., Kim D.-W., Fabbiano G., 2011, ApJ, 729, 12
Bregman J. N., Parriott J. R., 2009, ApJ, 699, 923
Brighenti F., Mathews W. G., Humphrey P. J., Buote D. A., 2009, ApJ, 705, 1672
Buitrago F., Trujillo I., Conselice C. J., Bouwens R. J., Dickinson M., Yan H., 2008, ApJ, 687, L61
Buote D. A., 2000, MNRAS, 311, 176
Canning R. E. A., Sun M., Sanders J. S., et al., 2013, MNRAS, 435, 1108
Condon J. J., Cotton W. D., Greisen E. W., et al., 1998, AJ, 115, 1693
Ferré-Mateu A., Mezcua M., Trujillo I., Balcells M., van den Bosch R. C. E., 2015, ApJ, 808, 79
Ferré-Mateu A., Trujillo I., Martín-Navarro I., et al., 2017, MNRAS, 467, 1929
Gaspari M., Brighenti F., Temi P., 2012, MNRAS, 424, 190
Gaspari M., McDonald M., Hamer S. L., et al., 2017, [arXiv: 1709.06564]
Gaspari M., Ruszkowski M., Oh S. P., 2013, MNRAS, 432, 3401
Gaspari M., Sądowski A., 2017, ApJ, 837, 149
Hilz M., Naab T., Ostriker J. P., Thomas J., Burkert A., Jesseit R., 2012, MNRAS, 425, 3119
Hlavacek-Larrondo J., Fabian A. C., 2011, MNRAS, 413, 313
Hogan M. T., McNamara B. R., Pulido F., et al., 2017, [arXiv: 1704.00011]
Irwin J. A., Athey A. E., Bregman J. N., 2003, ApJ, 587, 356
Kalberla P. M. W., Burton W. B., Hartmann D., et al., 2005, A&A, 440, 775
Lakhchaura K., Saini T. D., Sharma P., 2016, MNRAS, 460, 2625
Lodders K., Palme H., 2009, Meteoritics and Planetary Science Supplement, 72, 5154
Mathews W. G., Brighenti F., 2003, ARA&A, 41, 191
McNamara B. R., Nulsen P. E. J., 2007, ARA&A, 45, 117
McNamara B. R., Nulsen P. E. J., 2012, New Journal of Physics, 14, 5, 055023
Oser L., Ostriker J. P., Naab T., Johansson P. H., Burkert A., 2010, ApJ, 725, 2312
Parriott J. R., Bregman J. N., 2008, ApJ, 681, 1215
Pulido F. A., McNamara B. R., Edge A. C., et al., 2017, [arXiv: 1710.04664]
Quilis V., Trujillo I., 2013, ApJ, 773, L8
Rodriguez-Gomez V., Pillepich A., Sales L. V., et al., 2016, MNRAS, 458, 2371
Russell H. R., McNamara B. R., Edge A. C., Hogan M. T., Main R. A., Vantyghem A. N., 2013, MNRAS, 432, 530
Schure K. M., Kosenko D., Kaastra J. S., Keppens R., Vink J., 2009, A&A, 508, 751
Trujillo I., Ferré-Mateu A., Balcells M., Vazdekis A., Sánchez-Blázquez P., 2014, ApJ, 780, L20
van den Bosch R. C. E., Gebhardt K., Gültekin K., van de Ven G., van der Wel A., Walsh J. L., 2012, Nature, 491, 729
van der Wel A., Rix H.-W., Wuyts S., et al., 2011, ApJ, 730, 38
Voit G. M., Kay S. T., Bryan G. L., 2005, MNRAS, 364, 909
Walsh J. L., van den Bosch R. C. E., Gebhardt K., et al., 2017, ApJ, 835, 208
Werner N., Allen S. W., Simionescu A., 2012, MNRAS, 425, 2731
Werner N., Durret F., Ohashi T., Schindler S., Wiersma R. P. C., 2008, Space Sci. Rev, 134, 337
Werner N., Oonk J. B. R., Sun M., et al., 2014, MNRAS, 439, 2291
Werner N., Zhuravleva I., Canning R. E. A., et al., 2016, MNRAS, 460, 2752
Yıldırım A., van den Bosch R. C. E., van de Ven G., et al., 2015, MNRAS, 452, 1792